Studies on the Tempo of Bubble Formation in Recently Cavitated Vessels: A Model to Predict the Pressure of Air Bubbles[1]

Yujie Wang, Ruihua Pan, and Melvin T. Tyree*

College of Forestry, Northwest A&F University, Yangling, Shaanxi 712100, China

A cavitation event in a vessel replaces water with a mixture of water vapor and air. A quantitative theory is presented to argue that the tempo of filling of vessels with air has two phases: a fast process that extracts air from stem tissue adjacent to the cavitated vessels (less than 10 s) and a slow phase that extracts air from the atmosphere outside the stem (more than 10 h). A model was designed to estimate how water tension (T) near recently cavitated vessels causes bubbles in embolized vessels to expand or contract as T increases or decreases, respectively. The model also predicts that the hydraulic conductivity of a stem will increase as bubbles collapse. The pressure of air bubbles trapped in vessels of a stem can be predicted from the model based on fitting curves of hydraulic conductivity versus T. The model was validated using data from six stem segments each of *Acer mono* and the clonal hybrid Populus 84K (*Populus alba* × *Populus glandulosa*). The model was fitted to results with root mean square error less than 3%. The model provided new insight into the study of embolism formation in stem tissue and helped quantify the bubble pressure immediately after the fast process referred to above.

Vulnerability curves (VCs) have been viewed as a good measure of the drought resistance of woody stems (Cochard et al., 2013). Increasing drought increases the xylem tension (T) and eventually induces cavitation of the water in conduits when the T exceeds a certain threshold (Sperry and Tyree, 1988; Sperry et al., 1996). A cavitated vessel first fills with water vapor and eventually fills with air at atmospheric pressure because of Henry's law, which describes gas equilibrium at the water/air interface. The time required for the progress mainly depends on the penetration rate of air into the recently cavitated vessel lumen via diffusion through the liquid phase.

Previous studies were made about how fast bubbles disappear in embolized stems because of the solubility of air in water when water pressure exceeds atmospheric pressure, and the process takes 10 to 100 h depending on conditions (Tyree and Yang, 1992; Yang and Tyree, 1992). The tempo of bubble disappearance was measured by following the rise in stem hydraulic conductivity (k_h) versus time. The theory of Yang and Tyree (1992) relied on the same principles used in this article (Henry's law, Fick's law, and the ideal gas law), but modeling and experiments were done at pressures between 1 and 3 times atmospheric pressure rather than subatmospheric pressure (negative pressure). However, much less is known about the tempo of bubble formation in recently cavitated vessels (Brodersen et al., 2013). If the progress of embolus formation takes several minutes, then no changes in conductivity could be observed with available techniques, but if it takes hours, then the tempo of bubbles can be studied by rapidly inducing cavitation with increasing T and after cavitation induction measuring the influence of T on stem k_h as T is reduced gradually to zero. If air bubbles are at a pressure (bubble pressure [P_b^*]) lower than a threshold near atmospheric pressure, bubbles ought to collapse when T decreases according to the ideal gas law and Henry's law (see theory below). The consequence of bubble collapse will be partial filling of vessels with water and the rest with air bubbles. The partial filling of water in a recently cavitated vessel ought to increase the lumen conductivity from zero and connect the embolized vessel to adjacent conductive vessels and, hence, ought to increase the conductivity of the stem by an additional flow pathway (Wheeler et al., 2005; Hacke et al., 2006). The vascular system of stems is a complicated network with vessels of different lengths, diameters, and orientation (Evert, 2006), and the complex vessel network makes the additional pathway possible. Therefore, bubble collapse could be detected through the impact of T on the k_h of the stems in a way that is very similar to the methods used by Yang and Tyree (1992) but requires a more sophisticated centrifuge technique to induce embolism.

Many studies have assumed that the bubble pressure in newly cavitated vessels ought to be near atmospheric

[1] This work was supported by a 5-year 1,000-talents research grant (to M.T.T.).

* Address correspondence to mel.tyree@cantab.net.

The author responsible for distribution of materials integral to the findings presented in this article in accordance with the policy described in the Instructions for Authors (www.plantphysiol.org) is: Melvin T. Tyree (mel.tyree@cantab.net).

Y.W. performed most of the experiments, the modeling, and the data analysis; R.P. performed the general data analysis and the vessel parameters experiment; M.T.T. supervised the experiments and the modeling; Y.W. and M.T.T. wrote the article and the supplemental materials.

www.plantphysiol.org/cgi/doi/10.1104/pp.114.256602

pressure, and no corrections for bubble pressure have been taken in measuring percentage loss of conductivity (PLC) when T is lower than a critical threshold (Li et al., 2008; Wang et al., 2014a). As a result of bubble collapse, the measured k_h under a mild T should be higher than that under high T (greater than 0.5 MPa). And the lower the initial bubble pressure, the more bubbles collapse with decreasing T.

The aim of this study is to construct a model that estimates average bubble pressure in partly embolized stems from the functional dependence of k_h on T, and with this model, we can further our understanding of the tempo of bubble formation in stems. Here, we will argue that the tempo of bubble formation is in two phases: an initial rapid phase (seconds to minutes to complete) followed by a much slower phase (many hours to complete). Since there is no method for measuring the rapid phase, the rapid phase will be described theoretically below. Next, a theory will be developed that allows the estimation of the pressure of air in recently formed bubbles in vessels during the slow phase. An experimental validation of the model will follow that will yield values of bubble pressure within the first 1 to 2 h following the fast phase of embolism formation in vessels.

THEORIES AND MODELS

The Theory of Fast Embolus Equilibrium following Cavitation Events

Water-filled vessel lumina usually occupy about 10% (8.6% in *Acer mono* and 15.1% in Populus 84K [*Populus alba* × *Populus glandulosa*]) of the volume of wood. The remainder of the wood can be divided between air, water, and solids distributed between living and dead cells in woody xylem tissue; how much of the volume is air depends on prior history. Immediately following the rapid cavitation of a fraction (α) of the water volume (vessels), the vessel lumina will be filled primarily with water vapor. Some simple calculations demonstrate that, within a few seconds or minutes, a cavitated vessel will reach a quasi-stable pressure below atmospheric pressure by drawing from air dissolved in the immediate vicinity of the cavitated vessel. Three mechanisms are considered for air entry into a newly cavitated vessel: (1) the air derived from the dissolved air in the water of the cavitated vessel before the cavitation event happened, (2) mass flow through the pit pore that seeds cavitation, and (3) diffusion of air from surrounding tissue.

Based on the equilibrium partial pressure of water vapor above liquid water plus the solubility of air in water (Henry's law), the first mechanism contributes about 3.2 kPa of water vapor (at 298 K), 1.2 kPa of nitrogen, and 0.6 kPa of oxygen if the water in the embolized vessel is saturated with air and if all of it contributes to the embolus following the cavitation event. The nitrogen and oxygen partial pressures have to be viewed as upper bound estimates, because some of the dissolved air may be drawn up into the transpiration stream before it can escape into the cavitated vessel.

For the second mechanism, we can suppose that the mechanism of cavitation is air seeding from an adjacent vessel already filled with air. Air seeding is supposed to occur through the largest pit membrane pore at the T that is big enough to pull the air/water interface through a hypothetical pore of the pit membrane. If this pore remains filled with air following the cavitation event, then the pore could deliver air by pneumatic flow of air from the vessel that seeds the cavitation to the newly cavitated vessel. Calculation based on this model of pneumatic flow reveals that the process would take days to completely fill the cavitated vessel and, hence, can be ignored (Supplemental Appendix S1), and most researchers assume that the pore-seeding embolism will fill with water within seconds after the cavitation event.

The third mechanism requires us to invoke Henry's law to calculate how much air might be delivered from endogenous sources (from within the stem excluding the cavitated vessels). Here, we will assume that no air comes from exogenous sources (from outside the stem). First, we consider the final equilibrium from endogenous sources, then we will approximate the time to reach this early equilibrium. It is worth noting that the air in fibers and extracellular spaces may also be a major source of air in this progress; however, we followed the standard practice of flushing stems with degassed water to eliminate air in vessels and surrounding fibers. Solving Henry's law for a void forming a volume fraction α of space surrounded by air-saturated water yields the following relationship (Supplemental Appendix S1):

$$P_G = \frac{(1-\alpha)K_G P_G^*}{\frac{\alpha}{RT} + (1-\alpha)K_G} \quad (1)$$

where P_G is the partial pressure of gas species G at equilibrium, P_G^* is the partial pressure of nitrogen or oxygen in the atmosphere, K_G is the Henry's law constant of gas G, RT is the gas constant times Kelvin temperature, and α is the fraction of the water volume that has cavitated. The final bubble pressure in the embolized vessels should be $P_b^* = P_{O_2} + P_{N_2} + P_{H_2O}$, where P_{O_2} and P_{N_2} can be computed from Equation 1 and P_{H_2O} is the saturated water vapor pressure (3.2 kPa at 298 K). Figure 1 shows the relationship between α and the theoretical initial bubble pressure in stem. The curves in Figure 1 are upper bounded estimates of the early equilibrium pressure, because it is assumed that the surrounding water was saturated with air, as determined by P_G^* . But in the experiments presented below, stems were flushed with partly degassed solution, so the amount of gas in the surrounding tissue would have been below the saturation level (P_G^*).

The initial equilibration time was calculated using a simplified model for the diffusion of gas from a cylindrical shell surrounding recently cavitated vessels (Supplemental Fig. S1). Assume that α of the water volume instantly cavitated and that the cavitated

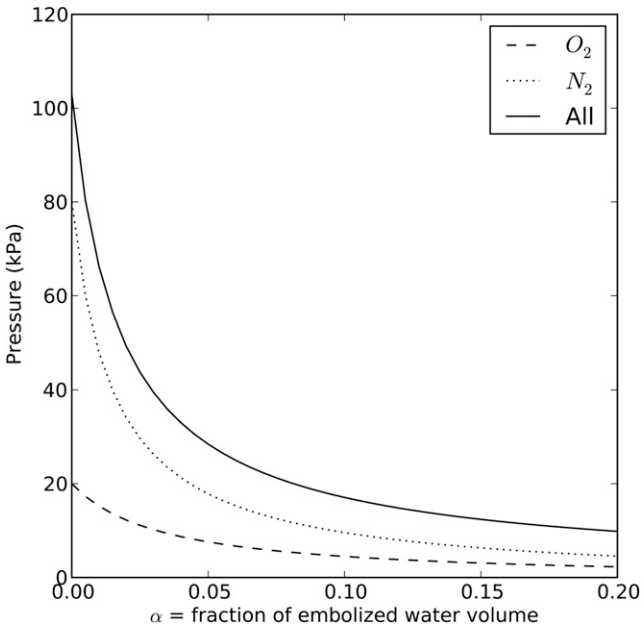

Figure 1. Relationship between the fraction of embolized water volume and partial pressure in the embolized vessels. The dotted line represents the partial pressure of nitrogen, the dashed line represents that of oxygen, and the solid line represents the sum of the partial pressure of oxygen, nitrogen, and saturated water vapor pressure (3.2 kPa at 298 K). This figure ignores the 1% contribution of argon to the gas mix in air.

vessels are evenly distributed throughout the stem. In a 1-cm segment of wood, each cavitated vessel of radius r would draw air from a cylindrical shell of water of radius R, such that the volume of the water shell = 1 cm $\pi(R^2 - r^2)\beta$ cm^3 of water, where β is the fraction of the wood volume that is water and $2R$ is the average distance between cavitated vessels. The maximum distance that air in solution would have to diffuse to the cell surface is $x = R - r$. The mean time t that it takes for half of the air molecules to diffuse through water at distance x is proportional to the distance squared: $x^2 = 2D_G t$, where D_G is the diffusion coefficient of gas species G in water (D_G of oxygen and nitrogen in water are 2.10E-5 and 1.88E-5, respectively). Using a typical value of vessel radius = 15 μm, α = 0.05 (5% of water embolized) and D_G can be assigned an estimated maximum distance of diffusion to be about $x \cong 55$ μm and the time for more than half the air to diffuse into the newly cavitated vessel to be ≅2 s, so 99% equilibrium would occur in less than 14 s (about six half-times). A more rigorous solution of the problem produced a result that was quite close to this estimate (Supplemental Fig. S2; Supplemental Appendix S1). If a smaller percentage of vessels cavitate, then the diffusion distance, x, for endogenous gas would be increased, making the t increase proportional to the square of x. For example, if 15% of the vessel cavitated instead of 50%, then x would increase by a factor of 3 and t would increase by a factor of 9.

We argue here that there should be a fast and a slow equilibrium phase. The fast phase is caused by localized equilibrium over a short x distance. By the time the fast equilibrium is completed, all subsequent Henry's law equilibrium has to be satisfied by diffusion over a much longer distance. For a 1-cm-diameter stem, this distance is roughly 5 mm (versus about 0.05 mm for the fast equilibrium) for air to diffuse from exogenous sources outside the stem. Since the time for equilibrium is proportional to the square of x, it follows that the slow equilibrium time will be $(5/0.05)^2 = 10^4$ times longer. So if the fast phase takes 10 s, the slow phase will be 10^5 s, or about 1 d.

In conclusion, we expect the initial equilibration of bubble pressure to be quite fast (10–100 s), depending on the percentage of vessels cavitated. In contrast, the time for exogenous sources of air (outside the stem) to diffuse into the stem should be much longer. The back of the envelope calculation in the previous paragraph suggests that this time is quite long. Some experimental validation about the time it might take can be gained from the time it takes air bubbles to dissolve in stems (Tyree and Yang, 1992). From tables 2 and 3 in Tyree and Yang (1992), it can be seen that the time for all bubbles to dissolve when the applied pressure is 14 kPa is about 150 h, and it is about 15 h when the applied pressure is 150 kPa for stems about the size used in the cavitron. If we equate full recovery to about three half-times, as measured by Tyree and Yang (1992), then the time for recovery will be up to 16 h near atmospheric pressure. We anticipated similar half-times for the reverse process of bubble formation. In the second article in this series, we measured the tempo experimentally, and the time needed was more than 1 d. The experimental conclusions of the above experiments were in agreement with theoretical models based on Henry's and Fick's laws.

Single-Vessel Model without *T* Gradients

The single-vessel model could be an ideal gas law model provided that the number of moles of gas in the bubble is constant. In this special case, the bubble volume (V_b) or bubble length (L_b) can be computed from absolute bubble pressure (P_b) and absolute water pressure (P_w) in or adjacent to the vessel. Assuming cylindrical geometry for vessels, we can say that:

$$\frac{V_b}{V_v} = \frac{L_b}{L_v} = \frac{P_b^*}{P_b} \tag{2a}$$

When the bubble completely fills the entire vessel, it has a pressure = P_b^* and it occupies the entire length of the vessel (L_v). As the bubble collapses to $L_b < L_v$, the bubble pressure increases ($P_b > P_b^*$) according to the ideal gas relation in Equation 2a. However, we have already argued above that gases quickly equilibrate between a vacuum void and surrounding tissue and that the equilibration time is generally less than 10 s

(for more exact solutions, see Supplemental Appendix S1). But the time required to do measurements of changes in k_h resulting from changes in L_b is much greater than 100 s. Bubble pressure will equilibrate with water adjacent to the bubble, and any increase in bubble pressure will result in the rapid movement of air from the bubble to the surrounding solution, which would invalidate the application of the ideal gas law. So we have to appeal again the Henry's law to explain changes in bubble size.

Taking into account Henry's law solubility together with the ideal gas law yields the following solution, where the numbers of moles of water and air are conserved in the vicinity of the embolus:

$$\frac{V_b}{V_v} = \frac{L_b}{L_v} = \frac{P_b^*}{P_b} - \left(\frac{1-\alpha}{\alpha} K_A RT\right)\left(\frac{P_b^*}{P_b} + 1\right) \qquad (2b)$$

with the restriction that $L_b \leq L_v$ if the right terms yield a larger value of L_b. Equation 2a is similar to Equation 2b except for the last term generated by Henry's law considerations, where α = the initial fraction of embolized volume with initial bubble pressure, P_b^*, and K_A is the equivalent Henry's law constant for air = a value based on 20% oxygen and 80% nitrogen. Equation 2b is maybe wrong by 1% or 2%, because it does not account for the amount of air/water entering the vessel as the bubble collapses. The bubble collapse could be a little more if water enters with air dissolved below the equilibrium concentration for P_b or could collapse less if the water that enters is more saturated with air. But in most solutions, the error will be just a few percentage points.

At final equilibrium, P_b should be higher than P_w because of the surface tension (γ) and contact angle (θ) between the water/air interface and the vessel wall of the lumen with diameter D_v. In this article, we assigned $\theta = 45°$ as typical, which ranged between 42° and 55° in various species (Zwieniecki and Holbrook, 2000). Hence, the bubble pressure is always higher than the water pressure by capillary pressure (P_C):

$$P_C = \frac{4\gamma\cos\theta}{D_v} \qquad (3a)$$

$$P_b = P_w + P_C \qquad (3b)$$

T is typically reported relative to barometric pressure (P_{baro}), whereas P_w is the absolute pressure; hence, we have $P_w = -T$ + barometric pressure, and hence:

$$P_b = -T + P_{baro} + P_C \qquad (3c)$$

The bubble pressure will change depending of changes in P_w (or T) and the number of moles of air in the bubble. In this article, the bubble volume change is computed by assuming that Henry's law equilibration happens continuously between P_b and the surrounding water.

The total resistance of a vessel (R_v) consists of lumen resistance (R_L) and pit resistance (R_P). The lumen resistance is proportional to the length of water in the lumen, while the pit resistance is proportional to the reciprocal length of water (Hacke et al., 2006). So, resistance of a vessel with L_v and water length (L_w) will be:

$$R_L = \frac{L_w}{L_v} \cdot R_{L,0} \qquad (4a)$$

$$R_P = \frac{L_v}{L_w} \cdot R_{P,0} \qquad (4b)$$

$$R_v = R_L + R_P \qquad (4c)$$

where $R_{L,0}$ and $R_{P,0}$ represent the lumen resistance and pit resistance of a nonembolized vessel, respectively. We use the generally accepted and empirical approximation that lumen resistance is equal to pit resistance in any vessel regardless of L_v (Hacke et al., 2006); hence, when we assume that $R_{L,0} = R_{P,0}$ and from Equations 4a, 4b, and 4c, we get:

$$R_v = \frac{L_v^2 + L_w^2}{2L_vL_w} \cdot R_{v,0} \qquad (5)$$

where $R_{v,0} = R_{L,0} + R_{P,0}$. The value of water length = $L_v - L_b$ can be substituted into Equation 5. If we want an expression for single-vessel conductivity ($k_{h,s}$), then by definition of conductivity and resistance $k_{h,s} = L_v/R_v$, we have:

$$k_{h,s} = \frac{2L_wL_v}{L_v^2 + L_w^2} \cdot \frac{L_v}{R_{v,0}} = \frac{2(L_v - L_b)\cdot L_v}{(L_v - L_b)^2 + L_v^2} \cdot \frac{L_v}{R_{v,0}} \qquad (6)$$

Ultimately, the value of $k_{h,s}$ depends on P_w or T. The conductivity of a stem segment can be equated to the sum of many $k_{h,s}$ values in series and parallel. When k_h is measured in a conductivity apparatus (gravimetric method; Li et al., 2008), P_w is above barometric pressure and it changes linearly with distance in the stem, so that embolized vessels at different locations in the stem would have only slightly different values of $k_{h,s}$. In contrast, if k_h is measured in a cavitron, then T or P_w is a quadratic function of radial position in the stem relative to the axis of rotation in the centrifuge (Cochard, 2002; Cai et al., 2010; Hacke et al., 2015), so the location of the vessel affects the value of P_w and, hence, the value of $k_{h,s}$ changes more dramatically with position, as shown in Figure 2. In this article, k_h of whole stems was measured in a centrifuge; hence, individual vessel $k_{h,s}$ values were modulated by changes in T near the vessel. Most readers can skip the detailed derivation of how k_h of a whole stem depends on the collective behavior of individual $k_{h,s}$ values in the cavitron (Supplemental Fig. S3; Supplemental Appendix S2), because the most important thing is to realize that k_h measured in a Cochard cavitron will change with the maximum tension at the center of rotation

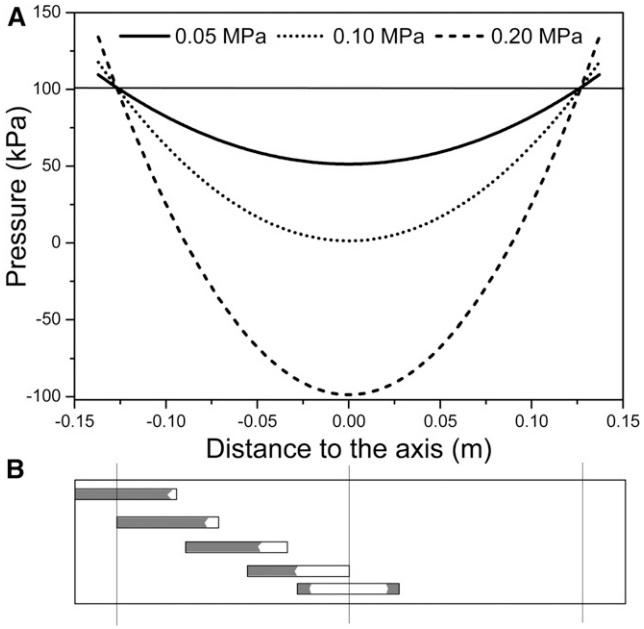

Figure 2. Pressure distribution in a cavitron and the pattern of bubble collapse due to pressure distribution. A, Absolute pressure distribution of three different T_c values: 0.05, 0.1, and 0.2 MPa. Average T values are always two-thirds of the T_c T. B, Bubble collapse in vessels located in different regions in stems.

(T_c) at the axis of rotation in a cavitron and that other values of T in the stem will be a quadratic function of T_c. Another important thing to remember is that T_c is consistently more than the average tension ($\overline{T}$) experienced by vessels. The ratio of $\overline{T}$ to T_c is always equal to 2:3.

The behavior of Equation 6 is plotted in Figure 3. When $T > P_{baro} + P_C - P_b^*$, the vessel lumen is fully embolized and the $k_{h,s} = 0$, but as soon as $T < P_{baro} + P_C - P_b^*$, the theoretical k_h begins to rise because of bubble collapse. Each curve in Figure 3 represents how k_h will change with T from low to high initial bubble pressure, P_b^*, in Henry's law equilibrium with surrounding tissue; at the three lowest bubble pressures, the bubble completely dissolves as T approaches 0. In contrast, at high P_b^* values, the bubble is only partly dissolved in the surrounding tissue. The reader should note that the recovery of conductivity happens only if the restored water in embolized vessels is adjacent to functional vessels. In a highly embolized stem, say PLC greater than 90%, this assumption may not be true, but for simplicity, we ignore this issue in the rest of this article. Addressing this real case would require specific knowledge of the three-dimensional interconnectivity of vessels, and such knowledge is not available.

RESULTS

Sensitivity Analysis of the Hydraulic Recovery Model

Standard sensitivity analysis of the model output (k_h) to the model parameters is needed to reveal which model parameters are most important in a hydraulic recovery curve (i.e. a plot of how much k_h increases in response to a decline in T_c). As discussed above and in Supplemental Appendix S2, we know that four parameters affect the final output of the model: (1) average bubble pressure, (2) fraction of embolized vessels in the stem, (3) L_v, and (4) vessel diameter, which determines the capillary pressure. The relationship between the model output and the parameters can be studied by keeping three of them constant while changing the fourth parameter.

Impact of the Bubble Pressure

According to the fast embolus equilibrium model, when the stem is under high T, say 1 MPa in the center, cavitated vessels will be filled with a mixture of water vapor and a subatmospheric partial pressure of nitrogen and oxygen. The model predicts that the k_h measured in a cavitron should increase as the centrifugal T decreases, because the bubbles will collapse in response to the rise of the P_w. The impact of initial bubble pressure on how the stem k_h changes with T is shown in Figure 4. Figure 4 also provides the theoretical basis for measuring bubble pressure through curve fitting, as explained in "Results."

According to the analysis in Figure 1, it seems likely that the initial P_b^* should be around 30 kPa when about 5% of the water volume is embolized (about 50% PLC, assuming that vessels make up 10% of the water volume). Figure 3 clearly shows that k_h should be nearly

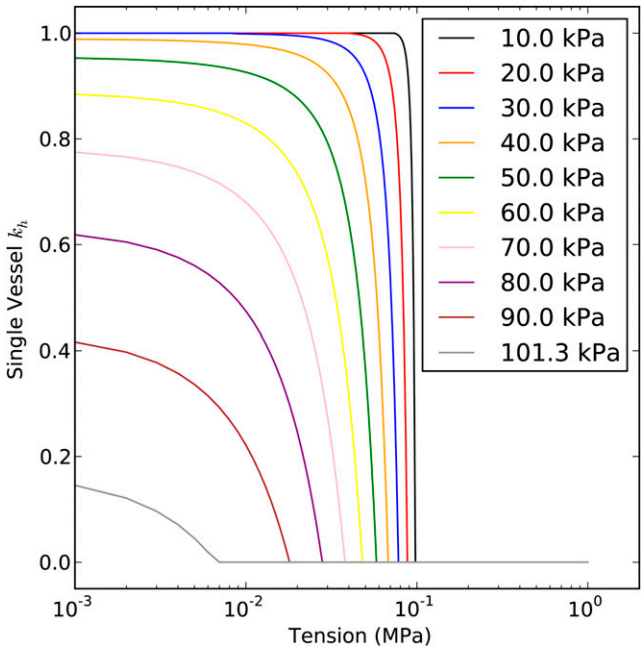

Figure 3. Solution of Equation 6. This single-vessel model shows how k_h changes with T. The y axis is the ratio of an embolized vessel to the k_h of a water-filled vessel. In this solution, P_C = 7 kPa and P_b^* was assigned values of 10 to 101.3 kPa, as shown in the key.

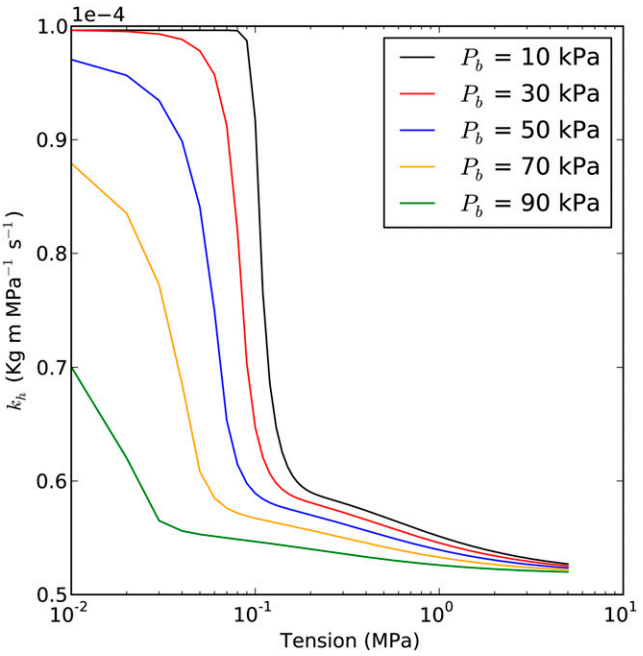

Figure 4. Prediction of the k_h curve versus T. Each curve is based on a different initial P_b^* value (10, 30, 50, 70, and 90 kPa) in the embolized vessels in the theoretical stem. Maximum k_h was set to 1E-4 kg m MPa^{-1} s^{-1} for each curve; average L_v was 5 cm; capillary pressure was 12 kPa; and the fraction of embolized vessels (ε) was 50% in the embolized segment (regions B–D in Supplemental Fig. S4, namely the portion of the segment that is not immersed in water).

independent of T_c until T_c fell below 0.2 MPa. Then, k_h sharply increased with decreased T_c from 0.2 to 0.01 MPa. The T axis is plotted on a log scale to display the data more clearly; otherwise, the plots would just show rapidly rising curves near the origin of the plot without much separation in the curves (plot not shown). The curves of k_h versus T_c rose faster in Figure 4 than in Figure 3 because, in a cavitron, the vessels far from the rotation axis were at lower T than near the axis of rotation, so the bubbles far from the axis start collapsing before the bubbles in vessels near the axis of rotation.

Impact of the Fraction of Embolized Vessels

Based on the argument in Figure 1 (Eq. 1), it seems unlikely that ε could change without P_b^* changing as well, since ε affects the fraction of embolized water, α. Figure 5 shows the prediction assuming that it is possible to change ε independently of P_b^*. It is worth noting that there should be a fairly close correlation between ε and the PLC observed at any given T_c.

Impact of L_v

Figure 6 demonstrated that the modeled value of k_h was relatively independent of L_v. This is probably because we assumed that lumen resistance and pit-membrane resistance were equal independent of the L_v, which agrees with the general empirical results (Hacke et al., 2006).

Impact of Vessel Diameter

Vessel diameter affects the capillary pressure in cavitated vessels; hence, it had some impact on the theoretical hydraulic recovery curve. According to Equation 3a, P_C is inversely proportional to vessel diameter. Figure 7 demonstrated that the maximum error caused by P_C is about 0.6% kPa^{-1}. Bubbles collapsed more with small-diameter vessels than with large-diameter vessels because of the higher values of P_C.

Experimental Results: Curve Fitting to Yield P_b^*

The hydraulic recovery model (Supplemental Appendix S2) was used to fit the results of six *A. mono* and six Populus 84K stems, as shown in Figures 8 and 9. The fitting involved finding the bubble pressure before bubble collapse, P_b^*, that minimized the root mean square error in the fitted line. The average root mean square error was generally less than 3%, as shown in Table I. The mean ± SD bubble pressure in Table I was 54 ± 14 kPa. All the bubble pressures estimated were lower than the atmospheric pressure.

The results of 12 fittings showed that more than 70% of the k_h change happened when the T_c was lower than 0.1 MPa. In terms of P_w, a T_c of 0.1 MPa corresponds to

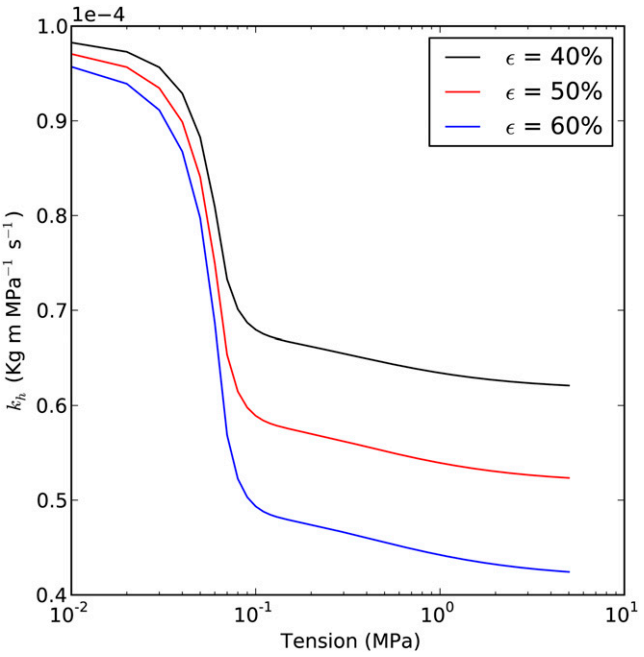

Figure 5. Prediction of the k_h curve with different values of ε. The relationship between PLC and the fraction of vessels cavitated is given by PLC/100 = ε. Each curve is based on a different ε value (40%, 50%, and 60%). Maximum k_h is 1E-4 kg m MPa^{-1} s^{-1}; average L_v is 5 cm; capillary pressure is 12 kPa; and P_b^* is 50 kPa.

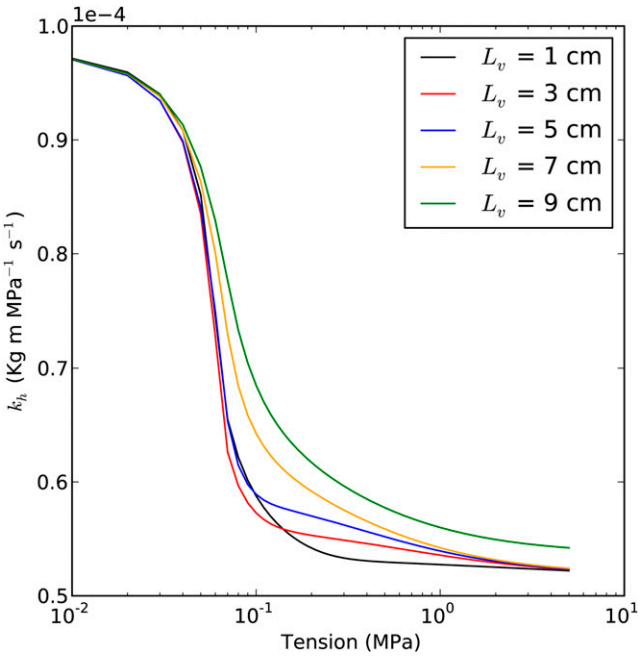

Figure 6. Prediction of the k_h curve with different average L_v values. Each curve is based on a different average L_v of the stem (1, 3, 5, 7, and 9 cm, as shown in the key). Maximum k_h is 1E-4 kg m MPa^{-1} s^{-1}; average P_b^*) is 50 kPa; capillary pressure is 12 kPa; and ε in the embolized segment is 50%.

P_w of 0 kPa. The k_h value was stable when T was higher than 0.3 MPa. On average, the k_h recovered 31% ± 8% and 68% ± 14% (means ± SE) of theoretical maximum recovery in *A. mono* and Populus 84K, respectively, when we decreased the T as shown in Figures 8 and 9. The minimum value of T_c used for measuring k_h was 0.045 MPa. The T profile is quadratic (Fig. 2), so T_c = 0.045 corresponded to a mean T of 0.030 MPa, because the mean was always two-thirds of T_c.

L_v and vessel diameter distributions measured in *A. mono* and Populus 84K are shown in Figures 10 and 11, respectively. *A. mono* had significantly shorter vessels at 2.851 ± 0.030 cm (n = 6) than Populus 84K at 5.797 ± 0.144 cm (n = 6). The mean vessel diameters were also significantly less in *A. mono* than in Populus 84K, 20.07 ± 0.09 μm (n = 3,575) versus 28.70 ± 0.11 μm (n = 4,307), respectively.

DISCUSSION

Impact of the Model Parameters and Estimation of P_b^*

Sensitivity analysis of our hydraulic recovery model revealed little impact of L_v on the determination of k_h. The estimated impact of using the mean L_v above rather than a L_v distribution biased our results by less than 0.1% (data not shown).

Vessel diameter distributions were as shown in Figure 11, and from Figure 7, we know that the maximum error caused by capillary pressure is 0.6% kPa^{-1}. Therefore, using the arithmetic mean of diameter generated a 0.09% error on the result compared with using a vessel diameter distribution (data not shown).

As shown in Figures 4 and 5, the primary factors controlling hydraulic recovery curves were P_b^* and ε. The value of ε was equated to the initial PLC at high T_c before the T was reduced (with the segment under water excluded). As the hydraulic recovery model predicted, the lower the P_b^*, the more bubbles collapsed and the more k_h recovered in a stem at constant ε values. As a result, the relative change of k_h was mainly determined by P_b^*. However, it must be remembered that P_b^* and ε are not totally independent of each other (Fig. 1; Eq. 1) after the fast phase of embolism formation.

Only the conductivity values measured in the cavitron were used to predict P_b^* in stems. Data used to fit k_h versus T curves cover a sufficient range of values to make accurate predictions of P_b^* (T_c from 0.032 to 1 MPa). Within the T range, k_h recovered 31% and 68% of the theoretical maximum recovery in *A. mono* and Populus 84K, respectively. The P_b^* calculated for Populus 84K was more accurate than for *A. mono*; but the likely error was not enough to alter the basic conclusion that, when cavitation was produced in a cavitron over a period of 1 h, relatively stable P_b^* resulted that was significantly less than the atmospheric pressure

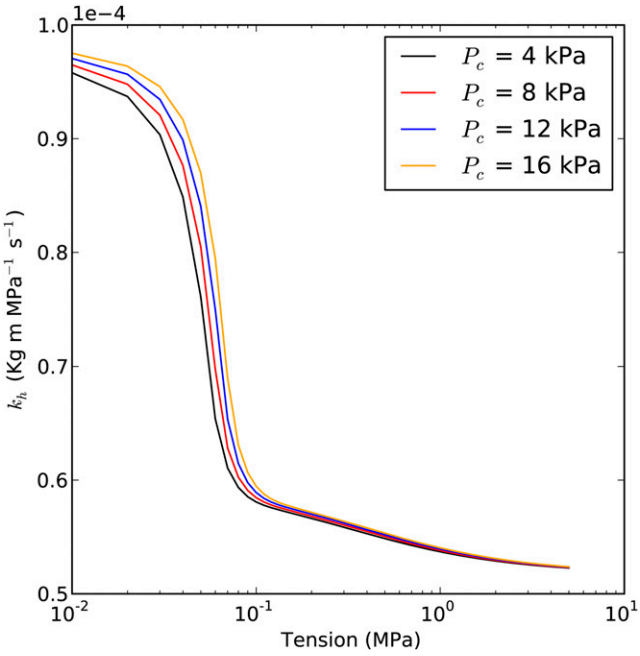

Figure 7. Prediction of the k_h curve with different P_C levels. Different P_C values (4, 8, 12, and 16 kPa) were used for each curve. Maximum k_h is 1E-4 kg m MPa^{-1} s^{-1}; average P_b^* is 50 kPa; average L_v is 5 cm; and ε in the embolized segment is 50%. The vessel diameter that corresponds to each P_C depends on cosθ ($\theta = \pi/4$). So the vessel diameters are 50.89, 25.44, 16.96, and 12.72 μm for P_C values of 4, 8, 12, and 16 kPa, respectively.

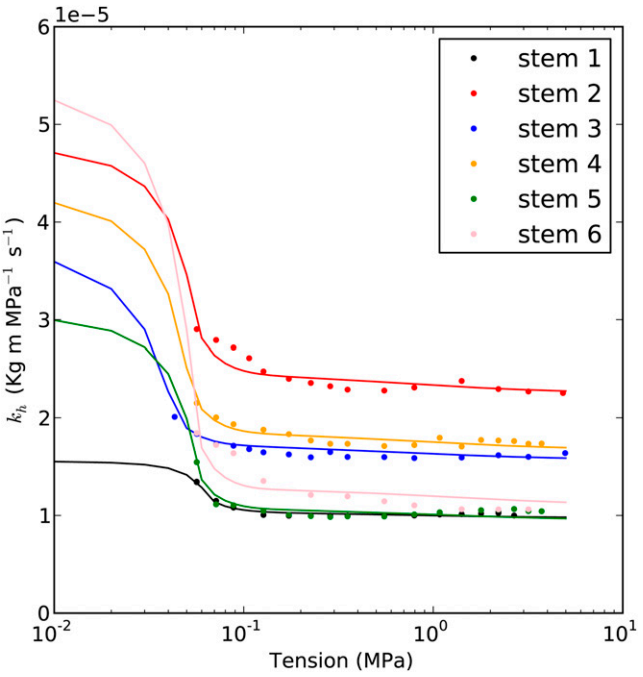

Figure 8. Examples of k_h curve fittings of *A. mono*. The circles are the k_h values measured in the cavitron, and the lines are the best fit curves. The details of the curves are as shown in Table I.

(100 kPa for the elevation of the university laboratory) based on Student's t test ($P < 10^{-4}$ for both species).

The purpose of this article was to present the hydraulic recovery model and show by curve fitting of data (k_h versus T) that values of initial bubble pressure can be derived from the fitted curves. The values of bubble pressure were higher than anticipated by us (54 kPa [Table I] versus about 35 kPa [Fig. 1]), but the reason for this will be explained in the next article in this series, where we measure the tempo of increase in P_b^*.

The Impact of Bubble Pressure on k_h and Vulnerability Curves

The model predicted that k_h will increase whenever T_c is decreased below about 0.3 MPa. The model results also predict that the lower the P_b^*, the more k_h depends on T. The value of k_h was most sensitive to decreases in T_c between 0.2 to 0.01 MPa. The results of *A. mono* and Populus 84K revealed that the model was validated by our data. Fitting the model to experimental data allowed the computation of P_b^* in embolized vessels. The hydraulic recovery model is an equilibrium model that indicates the final equilibrium, but it can be imagined that water has to flow into the stem to refill the vessels as the bubbles collapse; hence, we must address the issue of equilibration time to get an accurate value of k_h after a change in T.

Bubble collapse in stems involves the absorption of water into stems, and the water absorption will influence the k_h value measured in a centrifuge, resulting in an overestimation of k_h. The overestimation is a result of the assumption of steady state (i.e. that all water that enters the high-pressure end of the stem segment flows through to the low-pressure end). But if some of the water stays behind to fill part of the vessels (or other rehydrating regions), then the flow is overestimated at any given pressure drop, resulting in a k_h that is too high, as we measured the influx flow in a cavitron. Therefore, accurate measurement of k_h can be done only after this absorption process is completed. Preliminary measurements suggested to us that a 30-min wait was long enough to achieve stable k_h values at the smallest T_c = 0.03 MPa but became much faster as T_c increased. The water absorption also happens when the Sperry rotor is used to induce cavitation, and the standard protocol for k_h measurements in a conductivity apparatus is to correct the measurements of k_h for this background absorption rate (Hacke et al., 2000; Torres-Ruiz et al., 2012). In the following article of this series, a model of water absorption in the stem is presented, giving a better view of the kinetics of water absorption in stems due to bubble collapse.

Cochard (2002) and Li et al. (2008) both observed no difference in k_h measured in a stem at the target T_c versus the k_h measured later at a smaller T_c while stems were spinning in a centrifuge, using the original Cochard rotor or a functionally similar rotor fabricated by modifying a Sperry rotor (Li et al., 2008). Similar results were found during the testing of the Cochard

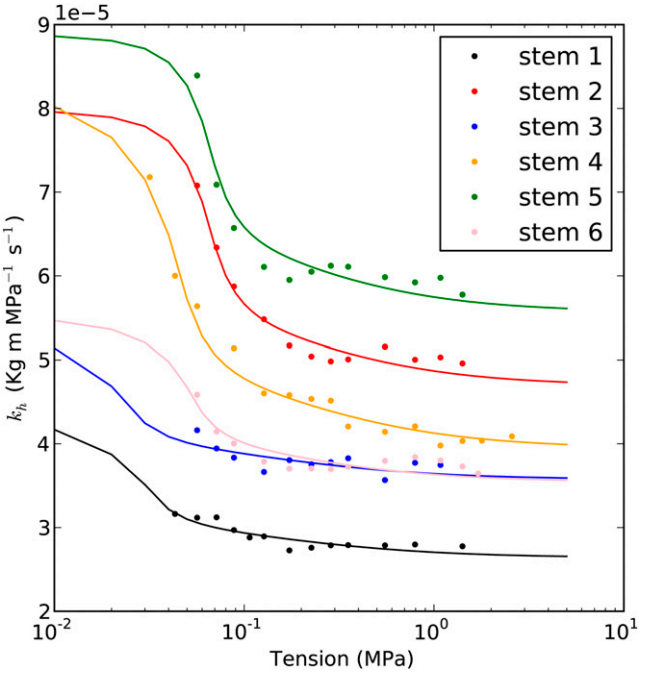

Figure 9. Examples of k_h curve fittings of Populus 84K. The circles are the k_h values measured in the cavitron, and the lines are the best fit curves. The details of the curves are as shown in Table I.

Table I. *Results of the k_h curve fitting of six A. mono stems and six Populus 84K stems*

k_{max} is the maximum k_h of the stem; cavitron PLC is the experimental PLC measured in a centrifuge; Sperry PLC is the PLC under atmospheric pressure predicted by the model; central PLC is the PLC at the central region of the stem predicted by the model; E_{RMS} is the route mean square error of the curve fitting; T_{form} is the time used to induce embolism in the stem; and $T_{recovery}$ is the total time used to measure the curve.

Parameter	Stem 1	Stem 2	Stem 3	Stem 4	Stem 5	Stem 6
A. mono						
k_{max} (E-5 kg m MPa^{-1} s^{-1})	1.57	5.02	4.28	4.69	3.28	5.96
Cavitron PLC (%)	39.55	57.00	65.88	66.08	72.60	82.70
Sperry PLC (%)	0.76	4.47	13.57	7.80	6.45	9.04
Central PLC (%)	42.66	61.49	71.07	71.28	78.32	89.21
P_b^* (kPa)	44.59	53.81	67.11	57.82	52.71	54.45
E_{RMS} (%)	1.77	2.78	1.60	2.20	4.58	4.03
T_{form} (h)	0.41	0.41	0.22	0.36	0.82	0.35
$T_{recovery}$ (h)	0.75	0.53	0.82	0.48	0.65	0.82
Populus 84K						
k_{max} (E-5 kg m MPa^{-1} s^{-1})	5.25	8.07	7.07	9.13	8.95	5.68
Cavitron PLC (%)	51.59	43.62	51.31	58.64	39.49	39.32
Sperry PLC (%)	16.12	0.92	21.95	9.16	0.65	2.54
Central PLC (%)	55.65	47.05	55.35	63.26	42.60	42.41
P_b^* (kPa)	57.76	72.45	34.45	37.25	77.44	38.48
E_{RMS} (%)	1.72	1.82	2.06	2.18	2.48	2.59
T_{form} (h)	0.56	0.20	0.47	0.53	0.26	0.49
$T_{recovery}$ (h)	0.77	0.33	0.48	0.82	0.27	0.29

cavitron in 2006 (M.T. Tyree, unpublished data). These observations contrast with the results of this article and deserve more analysis. In Li et al. (2008), no data were given, so the range of T_c over which k_h was measured was not given; in the earlier study (figure 4 in Cochard, 2002), it is clear that relative changes in k_h were measured from T_c = 1.8 to 0.1 MPa; this range should have been sufficient to detect the beginning of a trend (compare Figures 8 and 9), but the SE values of Cochard's early measurements were quite high (0.05–0.15), so no trend was detectable. The experiment has to be continued down to T_c = 0.03 MPa to discern the trend, and the trend has to be discerned in individual stem segments because the variance of the mean k_h is so large that it obscures the relationship. Proving the trends reported in this article also requires that k_h be measured with high precision on multiple measurements of k_h at a given T_c (SE < 0.02 and $n > 10$ is desirable). During the course of our investigation, techniques were improved; hence, some of the later experiments described here had higher precision values, with an SE closer to 0.004 in k_h (Wang et al., 2014b).

In our experiments, the minimum T used for the measurement of k_h ranged from 0.032 to 0.057 MPa, but during gravity-flow measurements, the applied water pressure is 2 to 3 kPa above barometric pressure (i.e. a T of -0.002 to -0.003). Using our model, we extended the theoretical calculations to include how positive pressure (negative T) would affect k_h measured by gravity flow. The results of these model calculations are reported in Table I (Sperry PLC). We compare the Sperry PLC with the average cavitron value (cavitron PLC) and the theoretical value near the axis of rotation (central PLC). The deviation of the theoretical Sperry PLC values compared with the cavitron PLC values in Table I is quite large and

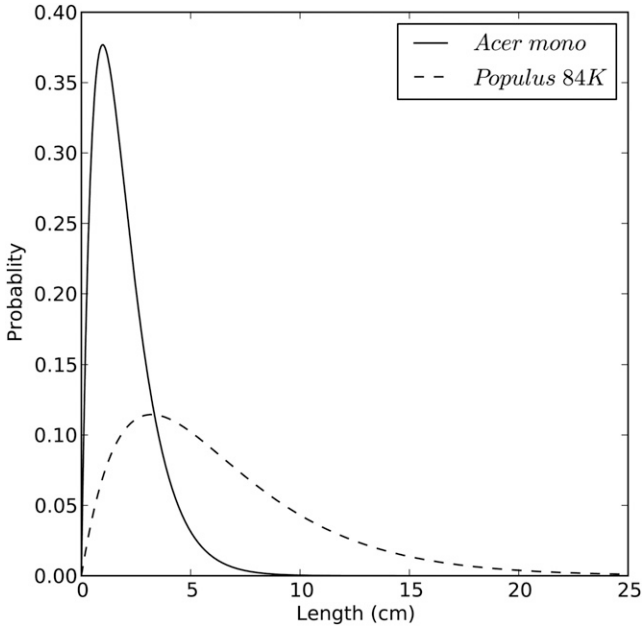

Figure 10. L_v distributions in *A. mono* and Populus 84K. L_v frequency was computed by using $P_x = k^2 x e^{-kx}$, where k is the extinction coefficient of the stem and x is the L_v. The values of k for *A. mono* and Populus 84K were 1.0246 and 0.3113, respectively.

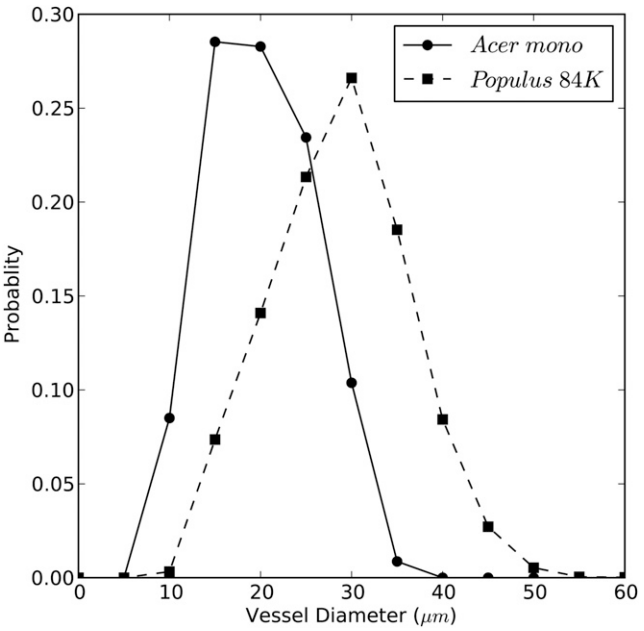

Figure 11. Vessel diameter distribution in *A. mono* and Populus 84K. The average diameters of *A. mono* and Populus 84K were 20.07 and 28.7 μm (arithmetic means), respectively.

probably the worst case possible, because the Sperry method arrives at the PLC values shown in Table I through various steps. In each step, the sample is spun to a higher T and then removed for measurement in a conductivity apparatus. After each k_h measurement in a conductivity apparatus, more air-saturated water is perfused through the stem, restoring the water-filled spaces near the vessels to a concentration near a saturated value (Henry's law). So when the stem is spun again, the quick equilibrium happens again and the bubble pressure of each embolized vessel would increase. In contrast, the model predicts what would happen if a high PLC were induced in a stem segment in one step and then moved immediately to a conductivity apparatus. Our model predicts that the Cochard VC will be different from the Sperry VC, but the stepwise measurements in the gravity method will make the bubble pressure rise to atmospheric pressure faster. Besides, the bubble collapse affected VC by decreased PLC (y axis), but T (x axis) was less affected because of the steep slope at P_{50} (for xylem pressure or tension at 50% loss of hydraulic conductivity). Therefore, no significant difference was observed between the two methods (Li et al., 2008).

In theory, the P_{50} (positive value) of a cavitron VC is lower than that of a Sperry VC (each point measured at equilibrium) because of the collapse of bubbles starting at a pressure less than 101.3 kPa (the standard atmospheric pressure at sea level). Even if the pressure is 101.3 kPa, there would be some collapse due to the impact of surface T on P_C and the 2% or 3% extra bubble compression resulting from gravity-flow measurements at 2 or 3 kPa above atmospheric pressure. But gravity-flow and cavitron-flow measurements are uncertain because of the uncertainty of temperature and stem rehydration. The measurement of k_h changes 2.3% °C^{-1} because of the influence of the temperature dependence of viscosity. Also, stems dehydrated in a centrifuge and then returned to a lower T or atmospheric pressure tended to rehydrate for the first 30 to 60 min, causing an overestimation/underestimation of flow and k_h unless care was taken to correct for rehydration affects. Readers should consult Torres-Ruiz et al. (2012) and Wang et al. (2014b) for methods of dealing with these problems in the gravity-flow method and cavitron method of measuring k_h, respectively.

CONCLUSION

In conclusion, the model predicts that the bubble pressure in recently cavitated vessels affects how much k_h changes with T_c in a cavitron. L_v and vessel diameter have little impact on the shape of hydraulic recovery curves (Figs. 5 and 6). The k_h increased due to the collapse of air bubbles in stems when the central T decreased, and the bubble pressure could be estimated by our model with an error of less than 3%. It is also worth noting that bubble collapse will not affect very much the value of P_{50} measured by Sperry's technique. This follows because bubble collapse influences most the y axis value of a vulnerability curve (PLC), but near P_{50} the curve is quite steep, so a large change in PLC results in a small change of the x axis value (T or negative pressure).

These models provide new insight into the tempo of bubble pressure and bubble formation in recently cavitated stems (i.e. that there should be a rapid rise in P_b^* within 1 min of cavitation followed by a much slower rise after 1 d). The next article of this series (Y. Wang, J. Liu, and M.T. Tyree, unpublished data) will more fully address the time needed for bubble pressure to rise in the slow phase of the equilibration with air external to the stem.

Table II. *The rpm and T_c in the cavitron we used*

The maximum rpm used for Populus 84K was 5,000, and that for *A. mono* was 7,000.

rpm	T_c	rpm	T_c	rpm	T_c
	MPa		*MPa*		*MPa*
500	0.022	1,400	0.173	4,000	1.415
600	0.032	1,600	0.226	4,500	1.791
700	0.043	1,800	0.287	5,000	2.211
800	0.057	2,000	0.354	5,500	2.675
900	0.072	2,500	0.553	6,000	3.184
1,000	0.088	3,000	0.796	6,500	3.736

MATERIALS AND METHODS

Branches (more than 1 m long) of a hybrid Populus 84K (*Populus alba* × *Populus glandulosa*) and *Acer mono* were sampled from and near the Northwest A&F University campus, and segments were excised while immersed in water. Segments with basal diameter of 5.5 to 7.5 mm were trimmed to 27.4 cm in length under water. The segments were flushed with 10 mM KCl for 30 min under pressure of 200 kPa (300 kPa absolute pressure). The liquid we used to flush the stem was filtered by a 0.02-μm filter and degassed under 40 kPa (absolute pressure) with a vacuum pump. Approximately 50% PLC was rapidly induced in a Cochard cavitron by spinning to a T of 2.2 MPa for Populus 84K and 4.2 MPa for *A. mono*. Then the central T was decreased to yield an absolute pressure higher than a perfect vacuum for at least 30 min (typically at 0.057 MPa in centrifuge T at the axis of rotation) to make sure that equilibrium was attained (i.e. that the period of water absorption had ceased). The k_h of the segments was measured from the low to high T values shown in Table II. Each T was held for 3 to 10 min until the stems were equilibrated (stable k_h measured). An improved regression method was used to calculate k_h to obtain a 4 to 5 times higher precision (Wang et al., 2014b). Preliminary experiments were done to determine how long T had to be held constant to get stable k_h values. These results indicated that 30 min was enough at 0.045 MPa and 3 to 10 min was enough for T values greater than 0.1 MPa.

Python(x,y) 2.7.5 was used to program the model, and the data acquired for k_h versus T_c was used to fit the model to estimate the average pressure of air bubbles in the stem by the least squares package in Python. The code for the model can be found in Supplemental Appendix S3.

Vessel Parameters

L_v was measured by the air-injection method described by Cohen et al. (2003) and Wang et al. (2014a). Briefly, long shoots were cut with a sharp razor blade and injected with compressed air at ΔP = 100 kPa (200 kPa absolute pressure) from the distal end; air was collected from the basal end immersed in water. Stem segments (20 cm long) were sequentially excised until bubbles were observed emerging from the distal end, and the flow rate of air bubbles ($Q = \Delta V/\Delta T$) was measured by water displacement. The stem was progressively shortened, and Q was measured at each length as above. The air conductance of cut-open vessels, C, was calculated from:

$$C = \frac{QLP}{A\Delta P\overline{P}}$$

as described by Cohen et al. (2003) and fitted into $C = C_0 \times e^{-kx}$, where C_0 is the maximum conductance as x approaches 0, k is an extinction coefficient, and x is the length of the stem. The k values were computed from the slope the curve of ln(C) versus x; and according to the theory of Cohen et al (2003), the most common L_v, L_{mode}, equals k^{-1} and mean L_v is calculated by $L_{mean} = 2L_{mode}$. Six stems were measured to calculate to average L_v of *A. mono* and Populus 84K.

Vessel diameters were measured on 25-μm-thick sections that were stained and photographed using a microscope (Leica DM4000B). Image-analysis software (Win CELL 2012; Regent Instruments Canada) was used to measure the diameter of hundreds of vessels, and arithmetic means were used to calculate capillary pressure by Equation 3a. Diameters were calculated from vessel area assuming circular geometry. The sum of vessel areas divided by wood area containing the vessels yielded values relative to the vessel fraction in both species.

Supplemental Data

The following supplemental materials are available.

Supplemental Figure S1. A model of cylindrical diffusion.

Supplemental Figure S2. The equilibrium time of cylindrical diffusion.

Supplemental Figure S3. Pressure equilibration in a vessel.

Supplemental Figure S4. The model of a stem in a cavitron.

Supplemental Appendix S1. Rapid equilibration of cylindrical diffusion.

Supplemental Appendix S2. A hydraulic recovery model.

Supplemental Appendix S3. The python code of a hydraulic recovery model.

ACKNOWLEDGMENTS

We thank Feng Feng for help in collecting samples and maintaining the flushing apparatus.

Received December 30, 2014; accepted April 22, 2015; published April 23, 2015.

LITERATURE CITED

Brodersen CR, McElrone AJ, Choat B, Lee EF, Shackel KA, Matthews MA (2013) In vivo visualizations of drought-induced embolism spread in *Vitis vinifera*. Plant Physiol **161:** 1820–1829

Cai J, Hacke U, Zhang S, Tyree MT (2010) What happens when stems are embolized in a centrifuge? Testing the cavitron theory. Physiol Plant **140:** 311–320

Cochard H (2002) A technique for measuring xylem hydraulic conductance under high negative pressures. Plant Cell Environ **25:** 815–819

Cochard H, Badel E, Herbette S, Delzon S, Choat B, Jansen S (2013) Methods for measuring plant vulnerability to cavitation: a critical review. J Exp Bot **64:** 4779–4791

Cohen S, Bennink J, Tyree M (2003) Air method measurements of apple vessel length distributions with improved apparatus and theory. J Exp Bot **54:** 1889–1897

Evert RF (2006) Esau's Plant Anatomy: Meristems, Cells, and Tissues of the Plant Body: Their Structure, Function, and Development, Ed 3. John Wiley & Sons, New York

Hacke UG, Sperry JS, Pittermann J (2000) Drought experience and cavitation resistance in six shrubs from the Great Basin, Utah. Basic Appl Ecol **1:** 31–41

Hacke UG, Sperry JS, Wheeler JK, Castro L (2006) Scaling of angiosperm xylem structure with safety and efficiency. Tree Physiol **26:** 689–701

Hacke UG, Venturas MD, MacKinnon ED, Jacobsen AL, Sperry JS, Pratt RB (2015) The standard centrifuge method accurately measures vulnerability curves of long-vesselled olive stems. New Phytol **205:** 116–127

Li Y, Sperry JS, Taneda H, Bush SE, Hacke UG (2008) Evaluation of centrifugal methods for measuring xylem cavitation in conifers, diffuse- and ring-porous angiosperms. New Phytol **177:** 558–568

Sperry JS, Saliendra NZ, Pockman WT, Cochard H, Cruiziat P, Davis SD, Ewers FW, Tyree MT (1996) New evidence for large negative xylem pressures and their measurement by the pressure chamber method. Plant Cell Environ **19:** 427–436

Sperry JS, Tyree MT (1988) Mechanism of water stress-induced xylem embolism. Plant Physiol **88:** 581–587

Torres-Ruiz JM, Sperry JS, Fernández JE (2012) Improving xylem hydraulic conductivity measurements by correcting the error caused by passive water uptake. Physiol Plant **146:** 129–135

Tyree MT, Yang S (1992) Hydraulic conductivity recovery versus water pressure in xylem of *Acer saccharum*. Plant Physiol **100:** 669–676

Wang R, Zhang L, Zhang S, Cai J, Tyree MT (2014a) Water relations of Robinia pseudoacacia L.: do vessels cavitate and refill diurnally or are R-shaped curves invalid in Robinia? Plant Cell Environ **37:** 2667–2678

Wang Y, Burlett R, Feng F, Tyree M (2014b) Improved precision of hydraulic conductance measurements using a Cochard rotor in two different centrifuges. Journal of Plant Hydraulics **1:** e-0007

Wheeler JK, Sperry JS, Hacke UG, Hoang N (2005) Inter-vessel pitting and cavitation in woody Rosaceae and other vesselled plants: a basis for a safety versus efficiency trade-off in xylem transport. Plant Cell Environ **28:** 800–812

Yang S, Tyree MT (1992) A theoretical model of hydraulic conductivity recovery from embolism with comparison to experimental data on Acer saccharum. Plant Cell Environ **15:** 633–643

Zwieniecki MA, Holbrook NM (2000) Bordered pit structure and vessel wall surface properties: implications for embolism repair. Plant Physiol **123:** 1015–1020

Supplemental details: Theory, models and Python code

Appendix 1: Rapid equilibration between air-saturated water surrounding newly cavitated vessels

(1) Final equilibrium of gas pressure

Henry's law states that the concentration C_G (mol·L^{-1}) of a gas species 'G' dissolved in water is in equilibrium with the partial pressure P_G^* of the gas species in air.

$$C_G = K_G P_G^* \tag{A1.1}$$

, where K_G (mol·L^{-1}·atm^{-1}) is the Henry's law constant.

If this is dissolved in a finite volume of solution, $(1-\alpha)V$, then the number of moles of solute n_s in solution is

$$n_s = (1-\alpha)VC_G = (1-\alpha)VK_G P_G^* \tag{A1.2}$$

The two main gases in Eq. A1.2 are O_2 and N_2 with K_G values of 1.3x10^{-3} and 8.1x10^{-4} respectively and the partial pressure of O_2 and N_2 in air are 0.21 and 0.78 atm. If a fraction, α, of volume V is embolized and no additional air is added to the system then n_s moles of gas will be divided into n_1 moles of gas in the cavitated volume and n_2 moles in the water such that $n_s = n_1 + n_2$.

If P_G is the partial pressure of gas in the cavitated volume (αV) then the ideal gas law can be used to yield

$$n_1 = \frac{\alpha V P_G}{RT} \tag{A1.3}$$

, where RT = the gas constant times Kelvin temperature, and the number of moles in the liquid will be given by

$$n_2 = (1-\alpha)VK_G P_G \tag{A1.4}$$

Equating Eq. A1.2 to A1.3 + A1.4 and solving for P_G yields Eq. 1 in the introduction.

$$P_G = \frac{(1-\alpha)K_G P_G^*}{\alpha/_{RT} + (1-\alpha)K_G} \tag{A1.5}$$

The atmosphere consists of about 78% nitrogen and 21% oxygen, hence the final equilibrium bubble pressure should be the sum of the equilibrium pressure of nitrogen, the equilibrium pressure of oxygen and a full vapor pressure, which is a function of

temperature (3.2 kPa at 298K).

(2) Diffusion time (cylindrical diffusion from bulk water)

The tempo of approach to equilibrium Eq. A1.5 can be computed by Fick's Law, which indicates that the radial diffusion rate of the gas species 'G' is proportional to the concentration gradient were diffusion occurs:

$$J_G = 2\pi D_G \cdot \frac{C_2 - C_1}{ln(b/a)} \quad \text{(A1.6)}$$

, Eq. A1.6 describes the diffusion in a unit length of cylinder where J_G is the diffusion rate in mol·s^{-1} per m of cylinder and D_G is the diffusion coefficient of gas; Eq. A1.6 describes the diffusion in a cylinder, where C_2 and C_1 are the concentration at the cylindrical surfaces with radius b and a, respectively (Crank, 1975).

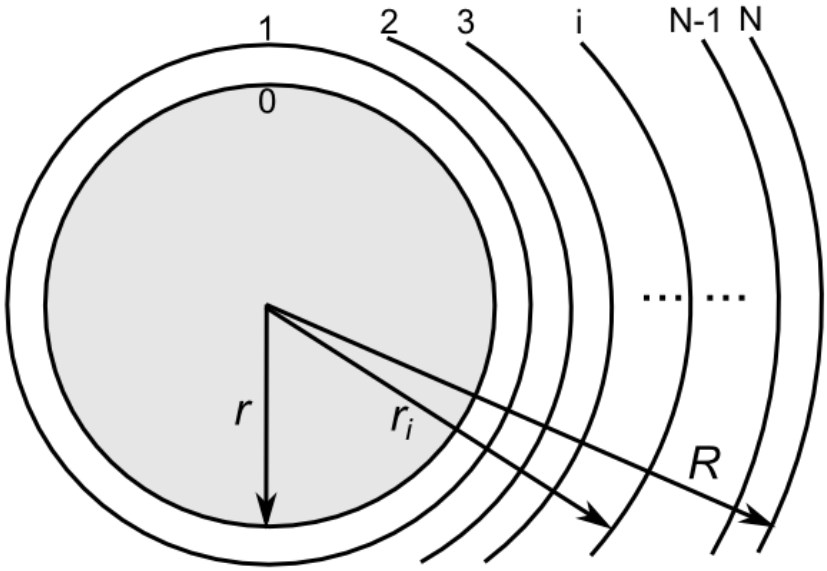

Figure S1. Model of cylindrical diffusion in stem. R and r are the radius of water (R = maximum radius) surrounding the vessel (r = vessel radius) , where r_i is the external radius of the ith layer of the N layers.

The cylinder was divided into N layers, each of which has a thickness of $\Delta x = (R - r)/N$. The boundaries of the ith layer of water $[r_{i-1}, r_i]$ are $[r + (i-1)\Delta x, r + i\Delta x]$; the

distance of half volume site of the layer to the center of the vessel, x_i, is $\sqrt{(r_{i-1}^2 + r_i^2)/2}$. At a time interval Δt, the gas diffusion rate in mol s^{-1} that diffuses out from the *i*th layer to *i-1*th layer will be:

$$\Delta n_i = 2\pi D_G \cdot \frac{C_{G,i} - C_{G,i-1}}{ln(x_i/x_{i-1})} \cdot L \cdot \Delta t \quad \text{(A1.7a)}$$

, where $C_{G,i}$ is the gas concentration of gas species 'G' in *i*th layer, which can be computed by Eq. A1.1, and $C_{G,0}$ is the equilibrium gas concentration in the cavitated vessel and L is an arbitrary length of the cylinder were diffusion occurs. Eq. A1.7 is used to compute the stem increase in dissolved gas concentration in the i^{th} cylindrical annulus in Fig. S1. The concentration change at *i*th layer would be $(\Delta n_{i+1} - \Delta n_i)/V_i$, where $V_i = 2\pi(r_i^2 - r_{i-1}^2)L$ so when this equation is substituted into A1.7 the value of L cancels out as does the 2π. So the equation for the increase in concentration in time step Δt is:

$$\Delta C_{G,i} = \frac{D_G \Delta t}{(r_i^2 - r_{i-1}^2)} \cdot [\frac{C_{G,i+1} - C_{G,i}}{\ln(x_{i+1}/x_i)} - \frac{C_{G,i} - C_{G,i-1}}{\ln(x_i/x_{i-1})}] \quad \text{(A1.7b)}$$

For initial condition at time 0 it is assumed that the cavitated vessel is filled with water vapor and the gases that were originally in the cavitated vessel before cavitation event happen (1.2 kPa N_2 and 0.6 kPa O_2). Therefore the gas pressure can be estimated by accumulating gas moles:

$$P_{G,t} = P_{G,t-\Delta t} + \frac{\Delta n_{1,t} RT}{2\pi r L} \quad \text{(A1.8)}$$

, where P_t and $P_{t-\Delta t}$ represent the gas pressure of gas species 'G' at time t and $t - \Delta t$ respectively, $\Delta n_{i,t}$ is the gas moles exchange in a time interval Δt at the time *t*.

The air pressure in vessels results from the combined diffusion of O_2 and N_2 which have different diffusion coefficients. Using an average vessel radius at 20 μm, the half time (T_{50}) and 99% equilibrium time (T_{99}) can be calculated and is shown in Fig. S2A, hence we can conclude that the initial bubble pressure can be reached in a short period of time.

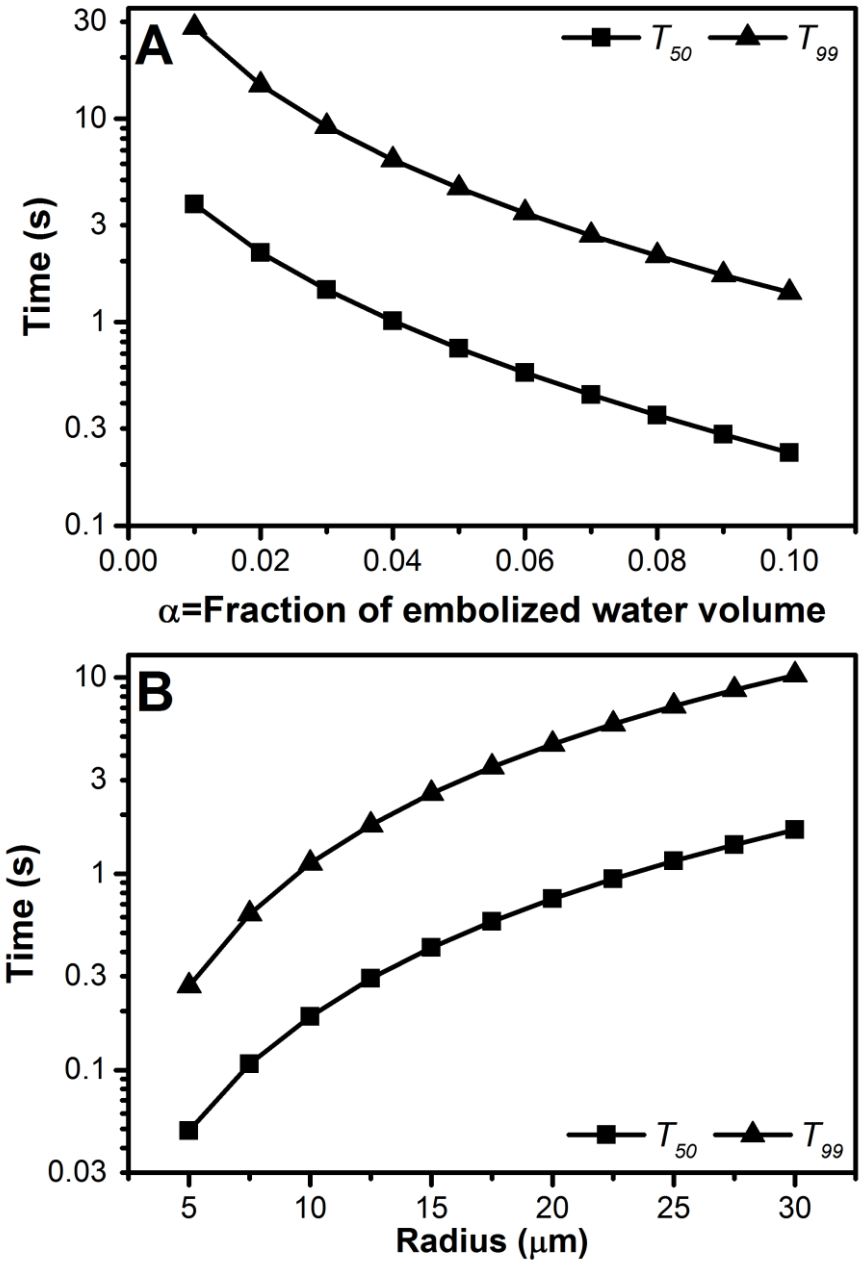

Figure S2. Relationship between α/radius and the half time and 99% equilibrium time. T_{50} and T_{99} refer to the half time (solid square) and 99% equilibrium time (solid triangle), respectively. Panel A: half time and 99% equilibrium time of the vessel with diameter of 20 μm when α range from 0.01 to 0.10. And in panel A α represents the fraction of embolized water volume in the stem. Panel B: half time and 99% equilibrium time of the vessel with diameter range from 5 to 30 μm when α is 0.05.

(3) Mass flow from the biggest pit pore

The following calculations demonstrate that mass flow of air through the biggest pit pore that seeds cavitation is very slow. According to the air-seeding hypothesis (Cochard et al., 1992; Sperry et al., 1996), an air bubble is pulled though the largest pit membrane pore connecting an embolized vessel to water-filled vessel. In this calculation let us assume the pore length, L, is 1 μm and the pore diameter, D, is 14.4 nm. A pore diameter this size would seed a cavitation at a tension of 2 MPa if the contact angle of the air-water interface with the pore wall is 0° and at lesser tension if the contact angle is >0°. This calculation assumes the pore remains filled with air and that pneumatic flow of air occurs indefinitely driven by the pressure difference between one vessel filled with air at atmospheric pressure to a recently cavitated vessel initially at 0 pressure.

Poiseuille's law for pneumatic flow is:

$$F_x = \frac{\pi\rho}{128\eta} \cdot D^4 \cdot \frac{dP_x}{dL} \quad \text{(A1.9)}$$

, where F_x is the mass flow rate ($Kg{\cdot}s^{-1}$), ρ is the density of air, η is the viscosity of air (which is nearly constant when P_x < 500 kPa). According to Cohen et al. (2003), the air conductivity can be computed by $C = {QLP}/{A\Delta P\bar{P}}$, where Q is the volume flow rate ($m^3{\cdot}s^{-1}$), L is the length of a pipe, A is the cross-section area of the pipe, P is the pressure where Q is measured, ΔP is the pressure difference across the pipe and $\bar{P}$ is the average pressure which equals to the mean of pressures at the two ends of the pipe (P_{in} and P_{out} below). So the atmospheric volume flow rate $F_{V,x}$ will be:

$$F_{V,x} = \frac{\pi D^4}{256\eta P_{baro} L} \cdot (P_{out}^2 - P_{in}^2) \quad \text{(A1.10)}$$

And the maximum flow rate $F_{v,max}$ will be the flow rate when P_{out} is P_{baro} and P_{in} is 0. And the volume of the vessel is $V_V = 0.25 \cdot \pi D_v^2 \cdot L_v$, where D_v and L_v are the diameter and length of the vessel. The average volumes of vessel lumen are 1.54E-11 m^3 (*Acer mono*) and 5.94E-11 m^3 (*Populus 84K*), and the maximum volume flow rate (at atmospheric pressure) are 2.89E-17 $m^3{\cdot}s^{-1}$ for both species on the assumption of same pit pore size. So the half time for an vacuum-filled vessel to obtain a bubble pressure about 50 kPa from the biggest pit pore will be $T_{half} = ln2 \cdot V_{vessel}/F_{V,max}$. And the T_{half} for an *Acer mono* vessel is about 3.1 days and T_{half} for a *Populus 84K* vessel is about 11.9 days.

Appendix 2: The Hydraulic Recovery Model: a model for estimating bubble pressure in vessels from measurements of stem k_h versus decreasing T_c in a cavitron.

The case of bubble pressure equilibrium in a vessel without pressure gradient has been discussed in Eq. 2 to 6 in the main paper. Below we discuss how the situation changes when there is a pressure gradient. The primary problem is to arrive at computational code that can transform Fig. 2 (the conductivity of a single vessel without a pressure gradient) to Fig 3 (the conductivity of many vessels in a stem segment in an environment with a quadratic pressure gradients), and also the case of linear positive pressure gradient. Linear pressure gradients arise when a conductivity apparatus is used in conjunction with a Sperry rotor whereas quadratic pressure gradients arise when measuring conductivity in a spinning Cochard rotor.

Once a computational algorithm is achieved for getting a stem segment conductivity, k_h, at any given initial bubble pressure (P_b^*) assigned at a high T_c values, the next step is use a curve fitting algorithm with root mean square error (E_{rms}) calculations to arrive at the value of P_b^* that best fits (minimizes E_{rms}) experimental data of k_h versus T_c for all the lower values of T_c during an experiment like those shown in Figs. 7 and 8.

(1) Pressure equilibrium between water and air in a single vessel with superimposed pressure gradient

In a centrifuge, there can be a static pressure gradient without flow of water wherein the most negative pressure occurs at the axis of rotation, and the pressure falls as a quadratic function of distance from the center ($P_w = \frac{x^2-R^2}{R^2} \cdot T_c + P_{baro}$, where x is the distance to the rotation axis). The centrifugal force will push the air bubble to the rotation axis hence the water will flow into the distal end of the vessel when $P_w + P_c > P_b$. In a conductivity apparatus (gravity flow system or flow meter), the water pressure will decrease linearly with distance in a stem and the bubble will tend to be oriented with the bubble at the low-pressure end of the vessel. However bubbles can ‘stick’ in small pipes

by a process similar to the static coefficient of friction so the bubble could be anywhere in the vessel although for simplicity it is illustrated at the low pressure end of the vessel.

In an embolized vessel that is filled with an air bubble at a pressure of P_b^* under high tension in centrifuge, the bubble will collapse when the tension is decreased and the pressure equilibrium is achieved as shown in Fig. S3, where the meaning of R_{dv} and L_w is defined. At any given pressure gradient, the water and bubble lengths (or volumes) in the cavitated vessel finally equilibrate. The water pressure can be computed by a quadratic function in Cavitron system and from a linear function in a conductivity apparatus; the bubble pressure can be obtained by applying the ideal gas law as in Eq. 2. Eq. A2.2a gives the linear pressure gradient in a conductivity apparatus, and Eq. A2.2b gives the quadratic pressure gradient in a cavitron.

$$P_w = P_0 - \lambda L_w \tag{A2.2a}$$

$$P_w = P_{baro} + \left(\frac{(R_{dv} - L_w)^2}{R^2} - 1 \right) \cdot T_C \tag{A2.2b}$$

, where λ is the coefficient of the pressure gradient, R is the maximum distance from the water level to the axis of rotation, P_w is the water pressure at the air/water interface at final equilibrium. The air bubble in the vessels are compressed hence the bubble pressure at final equilibrium P_b can be derived by the ideal gas law:

$$P_b = \frac{L_v}{L_v - L_w} \cdot P_b^* \tag{A2.3a}$$

. However, we have to take the air re-dissolved into the surrounding water as discussed in the main body. The equilibrium bubble pressure should be:

$$P_b = \frac{(1-\alpha) \cdot K_A + \alpha/RT}{(1 - \alpha + \alpha \cdot L_w/L_v) \cdot K_A + \alpha \cdot L_b/L_v \,/RT} \cdot P_b^* \tag{A2.3b}$$

where K_A is the Henry's Law constant for air and RT is the gas constant times Kelvin temperature. Therefore the final equilibrium in two systems can be given by:

$$P_0 - \lambda L_w + P_C = P_b \tag{A2.4a}$$

$$P_{baro} + \left(\frac{(R_{dv} - L_w)^2}{R^2} - 1 \right) \cdot T_C + P_C = P_b \tag{A2.4b}$$

, where P_C is the capillary pressure computed by Eq. 3a. Here Eq. A2.4a and A2.4b show the equilibrium of a vessel in Flow Meter system and Cavitron system, respectively.

Both the water pressure and bubble pressure are functions of L_w, hence we can solve

149 the functions to get the exact value of L_w. Newton iteration (details can be found on
150 Wikipedia) is used to solve Eq. A2.4a and A2.4b to get the L_w in any given vessel location
151 in a conductivity apparatus or centrifuge by assuming initial water length $L_{w,0} = 0$ and a
152 function of $f(L_w) = P_w - P_b$ at the beginning and then:

$$L_{w,i} = L_{w,i-1} + f(L_{w,i-1})/f'(L_{w,i-1}) \quad \text{(A2.5)}$$

153 , where $L_{w,i}$ and $L_{w,i-1}$ are the length of water at ith iteration, and L_w can be gained when
154 $L_{w,i} = L_{w,i-1}$. When pressure gradient $\lambda = 0$ and $P_0 = P_{baro}$ in a conductivity apparatus, L_w
155 can be calculated by Eq. A2.4b with the value of $T_C = 0$, and this is how the Sperry PLC
156 is simulated in Table I in the main body. Therefore, with Eq. A2.4 we are able to compute
157 any pressure equilibrium of a vessel at any vessel that begin at a known slice that is R_{dv}
158 far from the rotation axis, and hence to calculate the resistance of a cavitated vessel by
159 Eq. 5.

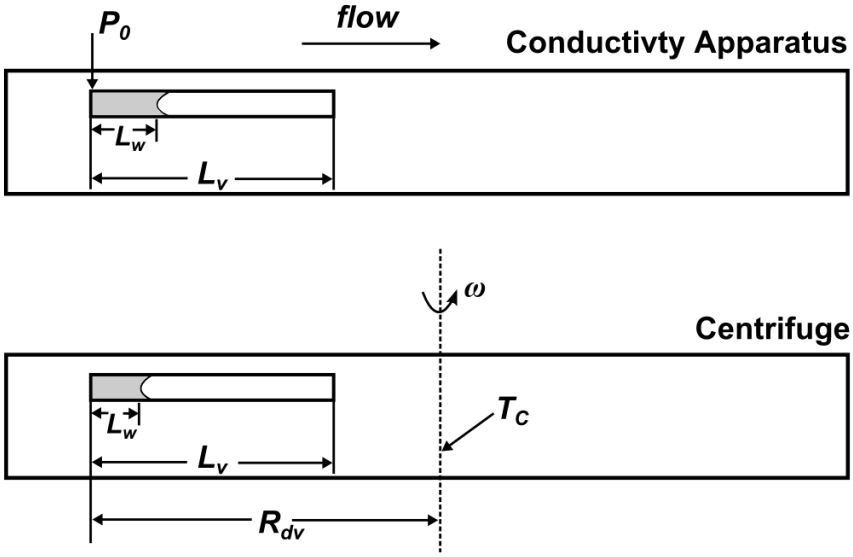

160

161 **Figure S3.** Model of water/air interface equilibrium in a single vessel. The upper panel
162 shows equilibrium of a vessel in a stem connected to a conductivity apparatus while the
163 lower panel shows equilibrium of vessel in a stem spun in a centrifuge. L_w and L_v
164 represent the length of water and vessel, respectively. In the upper panel, P_0 is the water
165 pressure at the upstream end of the vessel, and the pressure difference gradient is λ in
166 $kPa \cdot m^{-1}$; and the water finally equilibrates with bubble as in Eq. A2.4a. In the lower panel,
167 the central tension of the stem is T_C from angular speed ω, and the distance between the
168 distal end of the vessel and the axis of rotation is R_{dv}; and water equilibrates with bubble

as in Eq. A2.4b.

(2) Random vessel distribution and different equilibrium types

Vessels that are located in different places have different water pressure at the air/water interface and different bubble-length, so they have different final pressure equilibriums. Vessels are randomly distributed in stem such that any cross-section has the same possibility of vessel ends, vessel length distribution and vessel diameter. To make it simple, average vessel length and average vessel diameter were used to build the model instead of vessel-length distributions and vessel-diameter distributions.

As discussed above, in those vessels off the axis, bubbles are pushed towards the center because of the centrifugal force; but in those vessels that extend across the axis, water may enter from both ends and force bubble aggregate in the center as shown in Fig. S4. Air bubbles cannot exist in the sections of the stem immersed in water filled cuvettes (region a and e in Fig. S4). In our model the stem is divided into 5 parts: a, b, c, d and e as shown in Fig. S4; where a & e are immersed in water, c is the central region with length $2L_v$, and b & d are the remaining parts. When equilibriums are obtained in a Cavitron system, different computational algorithms apply based on different regions because of the vessel distribution. However, situation is simpler when segments are measured in a conductivity apparatus since bubbles tend to be pushed to the low-pressure ends, and hence Eq. A2.4a applies to the whole embolized segment.

In the Cavitron system, (1) in regions a and e, no air-seeding embolism can develop; (2) in regions b and d, equilibrium in normal type vessel can be given by Eq. A2.4b while end type vessel can be assumed as a normal type vessel with a shorter vessel length; (3) in region c, vessels can obtain equilibrium from one end just like the vessels in regions b/d, like vessel C_3 in Fig. S4; and can obtain equilibriums from both ends like vessels C_1 and C_2 in Fig. S4, and in this case the bubble length in these vessels is same as vessels that are symmetrically bisected by the rotation axis as vessel C_1 in Fig. S4. And the vessels like C_1 can be treated as two normal type vessels with length of $L_v/2$.

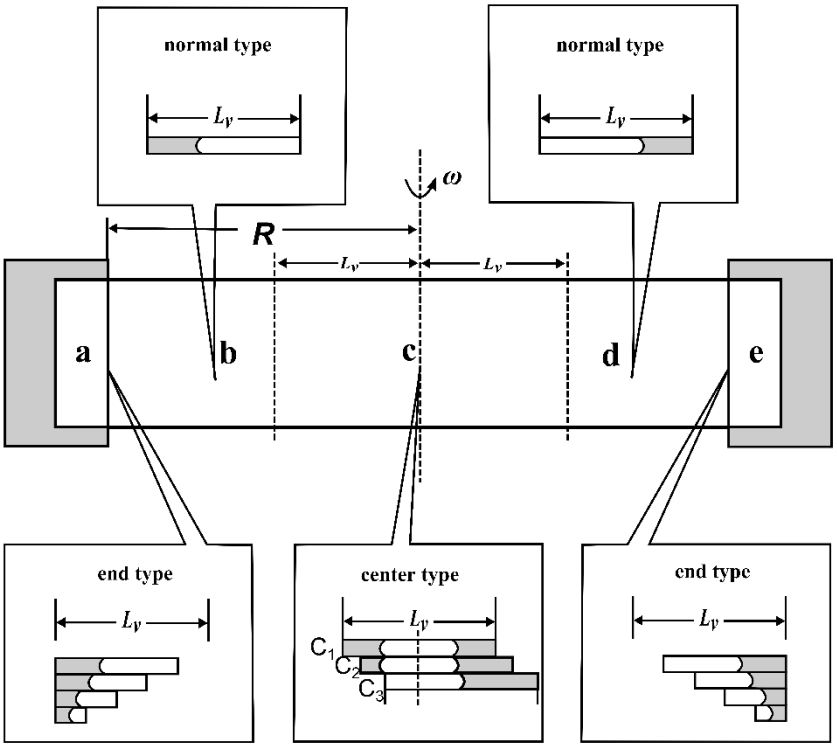

Figure S4 Model of stem divided into 5 regions and three types of cross-section. Five regions (a, b, c, d and e) are divided by the location and stature of vessels as described in Appendix 2.2. Three types of vessels (end, normal and center type) are defined based on the vessel location in any given slice. End type vessels are those that are open to the a/e boundaries, normal type vessels are those that locate between a/e boundaries and rotation axis, and center type vessels are those that cross the center.

(3) Stem model: adding up the resistances

Resistance of stem could be computed as $R_S=\sum R_{dx}\,dx$, where R_{dx} is the resistance of a dx-thick cross-section from the stem. To make it easy to understand, we use the average hydraulic recovery ratio of all the embolized vessels that pass through the slice to represent the hydraulic recovery ratio in the slice: $k = \sum k_i/N$, where k_i is the hydraulic recovery ratio of the ith vessel and N is the total number of vessels. So vessels are divided into three different type: end, normal and center types as described in Fig. S4.

Therefore, when equilibrium is obtained in end type vessels, the embolized vessel will recover its conductance by a ratio of $k = \frac{2l_w l_v}{l_w^2+l_v^2}$ (which follows from Eq. 5 in the main body), and here $l_v < L_v$ and l_w can be computed by Eq. A2.5. When equilibrium is obtained

in normal type vessel, embolized vessel recover its conductance by a ratio of $k = \frac{2l_w l_v}{l_w^2 + l_v^2}$, and here l_v is the average vessel length L_v and l_w is computed by Eq. A2.5. In those center type vessels where equilibrium can only occur from one end, embolized vessels recover conductance by the ratio of $k = \frac{2l_w l_v}{l_w^2 + l_v^2}$, here l_v is the average vessel length L_v and l_w is computed by Eq. A2.5. And in these center type vessels where equilibrium can occur from both ends, embolized vessels recover conductance by a ratio of $k = \frac{2l_w l_v}{l_w^2 + l_v^2}$, and here l_v should be $L_v/2$ and l_w should be computed by using $L_v/2$ as vessel length as described above. When equilibrium occurs from both ends in the vessels that are a little off the axis like vessel C_2, we can find that the length of bubble should be the same hence the resistance of the vessel should be the same with that of C_1, where the whole-length vessels behave like two vessels with length of $L_v/2$ that behave like normal type vessels that locate in b/d region, therefore the pressure equilibrium of a half-length vessel was used to represent the final equilibrium in center type vessels where equilibrium establishes from both ends.

In the slices in b/d, some of the vessels are open to the boundaries of a/e hence partial length vessels are used to compute hydraulic recovery ratio, together with the full length vessels to compute the average *k*. In the slices in c, some of the vessels are open to the center, hence equilibrium is able to form in two ends in which case can be treated as vessel C_1 in Fig. S4; and those vessels that are off the center and those that cross the center but with equilibrium only at one end can be treated as normal type vessels and share the same equation to compute *k*. And in this way, every embolized vessel that cross a given slice can be computed and then average *k* can be derived.

In a partly embolized stem, only $\varepsilon = n/N$ of the vessels out of a cross-section are cavitated or embolized (*n* is the number of cavitated/embolized vessels and *N* is the total number of all the vessels), and it was assumed that all vessels are of the same diameter and length. When water/air interfaces equilibrate with bubbles, the fraction of non-embolized vessels (1-ε) are fully conductive while the fraction of embolized vessels (ε) recover their conductivity by a ratio of *k*, and hence the conductivity of the slice is $[(1-\varepsilon) + k\varepsilon] \cdot k_{h,0}$, where $k_{h,0}$ is the conductivity of the slice with no embolism; and the

243 resistance of the cavitated vessels will drop as calculated from Eq. 5 and the resistance of
244 the slice will be computed by:

$$R_{dx} = \frac{1}{(1-\varepsilon)+k\varepsilon} \cdot R_0 \quad \text{(A2.6)}$$

245 , where R_0 is the resistance of the *dx*-thick slice when stem is fully conductive. Here
246 resistance rather than conductance is used because resistance can be added up directly in a
247 series of slices.

248 With the description above, the resistance of every *dx*-thick could be computed to
249 add up to the overall resistance of the stem by Eq. A2.6. We sacrifice some of the
250 accuracy of the model output in order to simplify some of the calculations and save
251 computational time which is currently about 20 minute per curve fitting. Future models
252 are worth developing with fewer sacrifices.

253 After all the resistances of *dx*-thick slices are calculated and added up at a given
254 tension, the total resistance of the stem is used to obtain the k_h of the whole stem under
255 different tensions by:

$$R_S = \sum R_{dx} \quad \text{(A2.7a)}$$

$$k_h = \frac{R_{S,0}}{R_S} k_{max} \quad \text{(A2.7b)}$$

256 , where $R_{S,0}$ is the resistance of the fully conductive stem, and k_{max} is the maximum
257 hydraulic conductivity of the stem.

258 *PLC* distribution in stems from centrifuges has been studied at slightly above
259 atmospheric pressure (Cai et al., 2010), but how *PLC* is distributed in segments spinning
260 in a rotor remains unknown because the bubble pressure of air in vessels in the
261 experimental conditions of Cai et al. (2010) is unknown. In this paper the fraction of
262 embolized vessels (ε) is assumed to be evenly distributed in stem between two reservoirs,
263 hence we assigned the same ε values in sections b, c and d under high tension while a and
264 e sections remain non-embolized (ε=0). In the second paper of this series other
265 distributions are considered and used to check how much the hydraulic recovery curve
266 could be influenced by different distributions of ε in stems spun in centrifuges.

267 In summary, the model assumes that (1) vessel length and vessel diameter were the

same in every vessel in the stem, (2) bubble pressure was the same in every cavitated vessel under high tension, (3) embolized vessel fraction ($\varepsilon = n/N$) was evenly distributed in b, c and d parts, and (4) contact angle in vessels was assigned to 45^{o} ($\pi/4$), which ranges from 42° to 55° (Zwieniecki and Holbrook, 2000). Based on these assumptions, the hydraulic recovery model is accomplished by: (1) calculated the resistance of a *dx*-thick slice, (2) added up the resistances of the stem, (3) computed hydraulic conductivity from resistances, and (4) calculate how hydraulic conductivity changes with decreasing tension.

The model was coded and run in Python(x,y) 2.7.5, the code can be found in the supplemental python script in Appendix 3.

Appendix 3: Python code of the Model

Note: The sentences after '#' are code descriptions, which will not run in python compiler. And to make it easy to read, we use a monospace font "Consolas" and landscape layout.

```
# range of central tension from 0.0 to 5.0 MPa
center_tension = []
tmptension = 0.0
while(tmptension <= 5.0):
    center_tension.append(tmptension)
    tmptension += 0.01

KCP_O = 1.30E-3 #mol.L-3.atm-1
KCP_N = 6.10E-4
KCP_A = 0.80*KCP_N + 0.2*KCP_O
RT = 298.0 * 0.0821 # atm.L.mol-1

def find_x(l,ct,bs):
    x = 0
    count = 0
    if (bs ** 2 / 0.127 ** 2 -1) * 1000 * ct + 100 + cp > BP:
        while 1:
            count = count + 1
            if(count >=20):
                x = l
                break
            fr = x / l
```

```
            fwt = 1.0 - center_PLC/100.0/10.0
            fbt = center_PLC/100.0/10.0
            fwe = fr*fbt + fwt
            fbe = fbt*(1.0-fr)
            funcKt = KCP_A*fwt + fbt/RT
            funcKe = KCP_A*fwe + fbe/RT
            EquilP = BP * funcKt/funcKe
            # judge here is Pw+Pc-Pb
            judge = ((abs(bs) - x) ** 2 / 0.127 ** 2 -1) * ct * 1000.0 + 100.0 + cp - EquilP
            # slope here is the slope of "judge" at x
            slope = - ct * 1000.0 / 0.127 ** 2 * 2.0 * (abs(bs) -x) + BP*funcKt/(funcKe**2) * (fbt/l*KCP_A -
fbt/RT/l)
            # Newton Iteration
            x = x - judge / slope
            #print judge,slope,x
            if (abs(judge) < 0.0001):
                # To judge when to stop
                break
            # A Statement to avoid overflow
            if x >= l or x < 0:
                x = l/1.2
    return x
# A function to compute the resistance of the embolized vessels at any given slice
def drawf_PLC(ct,vl):
    # Begin the slice array from the distal end of region a by the thickness of 0.001 m
    site = -0.137
```

```
    dsite = 0.001
    # Stop after the last slice at 0.137 m
    while(site < 0.138):
        # The resistance of slices in a/e is constant R0, we use R0=1.0
        if(abs(site) > 0.127):
            NEWR.append(1.0)
            OLDR.append(1.0)
        # The resistance of slices of end and normal type
        elif(abs(site) >= vl):
            klist = []
            ith = 1
            while(ith <= 100):
                tmpml = ith*0.01*vl + 0.127-abs(site)
                if(tmpml > vl):
                    tmpml = vl
                    tmpbs = abs(site) - (vl - ith*0.01*vl)
                    tmpwl = find_x(tmpml,ct,tmpbs)
                    tmpki = 2.0*tmpml*tmpwl / (tmpml**2 + tmpwl**2)
                    klist.append(tmpki)
                else:
                    tmpwl = find_x(tmpml,ct,0.127)
                    tmpki = 2.0*tmpml*tmpwl / (tmpml**2 + tmpwl**2)
                    klist.append(tmpki)
                ith += 1
            kr = numpy.mean(klist)
            NRdx = 100.0 / ((100.0-center_PLC) + kr*center_PLC)
```

```
            ORdx = 100.0 / (100.0-center_PLC)
            NEWR.append(NRdx)
            OLDR.append(ORdx)
        # The resistance of slices in region c
        else:
            klist = []
            ith = 1
            while(ith <= 100):
                tmpml = vl
                tmpbs = max(abs(site)+vl-ith*0.01*vl,abs(abs(site)-ith*0.01*vl))
                tmpes = min(abs(site)+vl-ith*0.01*vl,abs(abs(site)-ith*0.01*vl))
                if(abs(tmpbs) < vl):
                    # A judgement use to judge whether the equilibrium establish from both ends
                    ljudge = vl / (2*tmpes) * BP
                    # Patm = 100.0, Tension in MPa
                    rjudge = cp + ((tmpes/0.127)**2 - 1.0)*ct*1000.0 + 100.0
                    if(ljudge >= rjudge):
                        # When the slice is normal type slice
                        tmpwl = find_x(vl,ct,tmpbs)
                        tmpki = 2.0*tmpml*tmpwl / (tmpml**2 + tmpwl**2)
                        klist.append(tmpki)
                    else:
                        # When the slice is center type slice
                        tmpwl = 2.0 * find_x(vl/2.0,ct,vl/2.0)
                        tmpki = 2.0*tmpml*tmpwl / (tmpml**2 + tmpwl**2)
                        klist.append(tmpki)
```

```
                else:
                    tmpwl = find_x(vl,ct,tmpbs)
                    tmpki = 2.0*tmpml*tmpwl / (tmpml**2 + tmpwl**2)
                    klist.append(tmpki)
                ith += 1
            kr = numpy.mean(klist)
            NRdx = 100.0 / ((100.0-center_PLC) + kr*center_PLC)
            ORdx = 100.0 / (100.0-center_PLC)
            NEWR.append(NRdx)
            OLDR.append(ORdx)
        site += dsite

# Main Body of the Code
# cp here is actually capillary pressure
# Here we use lists to store the values of each parameter
cps = [7.0,]
vessel_lengths = [0.04,]
filenames = ["./Test.txt",]
Kmaxs = [1.0E-4,]
cPLCs = [50.0,]
BPs = [50.0,]
# main part
for i in range(len(filenames)):
    # Assign the parameters!
    OLDR = []
    NEWR = []
```

```
    savefilename = filenames[i]
    kmax = Kmaxs[i]
    center_PLC = cPLCs[i]
    BP = BPs[i]
    cp = cps[i]
    vessel_length = vessel_lengths[i]
    savefile = open(savefilename,"w+")
    savefile.write("Tension\tKh\tPLC\n")
    # Here we give a limit to vessel length to avoid overflow
    if vessel_length < 0.127:
    #cycle through center tensions
        for tension in center_tension:
        # Clear OLDR,NEWR in each cycle
            OLDR = []
            NEWR = []
            # Compute the resistance in 275 slices
            drawf_PLC(tension,vessel_length)
            tmpkh = kmax * (274.0 / sum(NEWR))
            tmplc = 100.0 - 100.0*(274 / sum(NEWR))
            tmpstr = str(tension) + "\t" + str(tmpkh) + "\t" + str(tmplc)
            print tmpstr
            savefile.write(tmpstr + "\n")
    # Save the output results and close the file
    savefile.close()
```

LITERATURE CITED

Cai J, Hacke U, Zhang S, Tyree MT (2010) What happens when stems are embolized in a centrifuge? Testing the cavitron theory. Physiol Plant **140:** 311-320

Cochard H, Cruiziat P, Tyree MT (1992) Use of Positive Pressures to Establish Vulnerability Curves - Further Support for the Air-Seeding Hypothesis and Implications for Pressure-Volume Analysis. Plant Physiol **100:** 205-209

Cohen S, Bennink J, Tyree M (2003) Air method measurements of apple vessel length distributions with improved apparatus and theory. J Exp Bot **54:** 1889-1897

Crank J (1975) The mathematics of diffusion. Clarendon press Oxford

Sperry JS, Saliendra NZ, Pockman WT, Cochard H, Cruiziat P, Davis SD, Ewers FW, Tyree MT (1996) New evidence for large negative xylem pressures and their measurement by the pressure chamber method. Plant Cell Environ **19:** 427-436

Zwieniecki MA, Holbrook NM (2000) Bordered pit structure and vessel wall surface properties. Implications for embolism repair. Plant Physiol **123:** 1015-1020